Indian Journal of Geo Marine Sciences
Vol. 49 (02), February 2020, pp. 184-191

Using an Artificial Neural Network for Wave Height Forecasting in the Red Sea

Khalid M. Zubier

Marine Physics Department, Faculty of Marine Sciences, King Abdulaziz University, P.O. Box 80207, Jeddah 21589, Saudi Arabia

*[E-mail: kzubier@kau.edu.sa]

Received 23 July 2018; revised 19 September 2018

Artificial Neural Networks (ANNs) are widely used in the field of wave forecasting as data-based soft-computing techniques that do not require prior knowledge regarding the nature of the relationships between the forecasted waves and the controlling physical mechanisms. Among ANN-techniques is the Nonlinear Auto-Regressive Network with eXogenous inputs (NARX), based on which two models were developed in this study to predict the significant wave heights in Eastern Central Red Sea for the next 3, 6, 12 and 24 h. The two NARX-based models differ only by the inclusion of the variance between wind and wave directions in one model and not in the other. Both models have shown the ability to efficiently predict the significant wave heights up to 12 hours in advance. However, the outperformance of the model that included the difference between wind and wave directions indicated the significance of the inclusion of such an input term.

[Keywords: Artificial neural network (ANN); Non-linear auto-regressive network with eXogenous inputs (NARX); Red Sea; Wave Forecasting**]**

Introduction

Wind generated waves can have significant impacts on navigation, shoreline structures and coastal marine environments. Long-term wave hindcasting and relatively short-term wave forecasting are important procedures to obtain wave information required to minimize such impacts. For locally generated waves, wave parameters can be hindcasted using empirical formulas, such as those given in Shore Protection Manual[1], Guide to Wave Analysis and Forecasting[2] and Coastal Engineering Manual[3], based on the local wind speeds. Furthermore, local wind speeds can also be utilized to obtain wave spectrum using more sophisticated empirical formulas, such as Pierson-Moskowitz Spectrum[4], JONSWAP Spectrum[5], and TMA Spectrum[6,7]. The propagation of the wind generated waves can be simulated using phase-resolving and phase-averaging numerical wave models[8,9]. Phase-averaging numerical models such as WAM[10], SWAN[11] and WAVEWATCH III[12] are based on energy balance (or action balance in the presence of currents) equation and are widely used, nowadays, to simulate wave generation, propagation and energy transformation. Performance of all these numerical models depends mainly on the quality of the input wind filed representing the forcing function for such models as well as the ability of the models to account for the associated physical mechanisms. The spatial and temporal resolutions of the forcing wind filed can significantly affect the quality of the wave field simulation[13,14].

Artificial Neural Networks (ANNs) are soft-computing techniques whose core is represented by an imitated design of human neurons that are utilized (as a network) in the development of cognitive algorithms to mimic the functioning of the human brain[15]. These algorithms train the network through learning processes to allow for the approximation of the actual mathematical behavior without any beforehand assumption of the interrelations between the input and output data. The learning processes involve continuous adjusting of weights and biases within the hidden layer that connects the input and output layers in a typical 3 layers ANN structure. Previous studies[16-18] have provided extensive reviews of ANN applications in the different fields of ocean engineering. In terms of wave prediction, several studies[19-26] have demonstrated the efficiency of ANN techniques. In addition, other studies[27-30] have shown the superiority of ANN techniques in wave prediction when compared with other soft-computing techniques.

Nonlinear Auto-Regressive Network with eXogenous inputs (NARX) is a dynamic ANN in which the output depends on both the current input to the network and the previous input and output, therefore, it is classified under Recurrent Neural Network (RNN) type[31,32]. This soft-computing

technique, NARX, has been used in wave height forecasting/prediction. Based on calculated correlation coefficients, one study[33] showed that using NARX yields better results, in terms of wave height forecasting, than the previous neural network applications by other researchers. Another study[34] used correlation coefficients as indicator to show the better performance of NARX, in comparison to Feed-Forward Back Propagation Network (FFBP), in wave height prediction.

The Red Sea is considered as one of the most economically important water bodies, judged by the high volume of navigation including commercial shipping and oil tankers transportation. In addition, the Red Sea is characterized by a unique marine environment that countries located on the Red Sea are striving to protect and conserve as a source for water and food security. The Red Sea can experience occasional energetic wave conditions due to strong monsoonal winds. Using SWAN model, several studies[35-38] simulated the observed wave conditions in the Red Sea. In other studies[39-46], WAVEWATCH III model was used to simulate the Red Sea wave conditions. The validation/verification procedures, using conventional wave buoy/rider measurements and satellite-based wave measurements, have indicated the good performance of these two spectral wave models. The wave measurements obtained using Thual Met/Ocean Buoy (NDBC: 23020), located on the central eastern side of the Red Sea, have been used by most of the above mentioned studies for model verification.

In this study, two NARX based models were developed to predict the significant wave heights at Thual Met/Ocean Buoy location with different forecasting horizons (3, 6, 12, and 24 h). In both models, the input layer contains time delayed wind data and fed-back wave data. The only difference between the two models is the inclusion of the variance between wind and wave directions in one model (B) and not in the other model (A). This allowed for the determination of the role played by the directional difference on the overall performance. As the first study using ANN to predict waves in the Red Sea, this study attempts to encourage other researchers to carry on future work along this line of research in a sea that is apparently lacking in terms of conventional wave measurements and operational wave predictions.

Materials and Methods

Thual met/ocean buoy (NDBC: 23020) was deployed offshore Thual, in the eastern central Red Sea (Fig. 1) at (22°9'43" N 38°30'0" E) where water depth is 693 m, by King Abdullah University for Science and Technology (KAUST). More than 10 months (2009/11/24 – 2010/09/18) records of hourly wind (speed and direction) and wave (height and direction) data were used in this study. From these records, the following two data sets were generated:

Set (A): (U_*, H)

Set (B): $(U_* cos(\varphi - \theta), H)$

where U_* is the wind shear velocity, H is the significant wave height, φ is the wind direction, and θ is the mean wave direction.

The wind shear velocity was calculated based on the following equation:

$$U_* = U_{10} \sqrt{C_D} \quad \ldots (1)$$

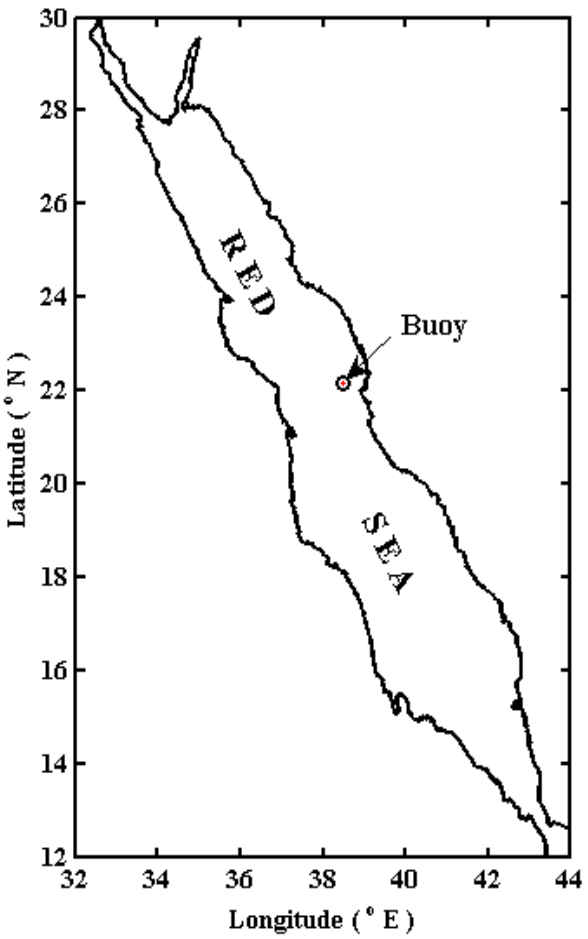

Fig. 1 — Red Sea map with location of Buoy shown as red circle.

where C_D is the wind drag coefficient which varies with the 10 meter wind speed U_{10} according to the following:

$$C_D \begin{cases} 1.2875 \times 10^{-3} & for\ U_{10} < 7.5\ m/s \\ (0.8 + 0.065 \times U_{10}) \times 10^{-3} & for\ U_{10} \geq 7.5\ m/s \end{cases} \quad \ldots (2)$$

NARX is a type of ANN that is utilized in time series analysis to efficiently recognize the non-linear relationships between temporal data. The most common NARX architecture (Figure 2) consists of three layers: Input, Hidden and Output. The input layer contains number of neurons that are fed-forward with specified time-delay, while the output layer contains a single neuron. The hidden layer, which falls in between the input and the output layers contains selected number of hidden neurons. With this architecture, the following two NARX-based models were developed in this study:

Model (A):

$$H_{t+i} = f(U_{*t}, U_{*t-1}, U_{*t-2}, H_t, H_{t-1}, H_{t-2}) \quad \ldots (3)$$

Model (B):

$$H_{t+i} = f(U_{*t}\cos(\varphi - \theta), U_{*t-1}\cos(\varphi - \theta), U_{*t-2}\cos(\varphi - \theta), H_t, H_{t-1}, H_{t-2}) \ldots \quad \ldots (4)$$

where t represents the time and i represents the forecasting time horizon of 3, 6, 12 and 24 h.

The utilization of wind shear velocity as an input rather than the wind speed (U_{10}) was based on the comparison made by another study[29], which showed that using the wind shear velocity yields more accurate results. That same study also recommended the inclusion of the cosine-shaped function $\cos(\varphi - \theta)$ in modeling to account for the difference between the wind and wave directions which could have an important role.

Each data set (A and B) was divided into two sub-sets, 80 % for training and 20 % for testing. For training purposes, three backpropagation training functions (Levenberg–Marquardt, Bayesian Regularization and Scaled Conjugate Gradient) were applied to each model and performances were compared. For both models, the comparison clearly showed that better performance was obtained using the Bayesian Regularization training function.

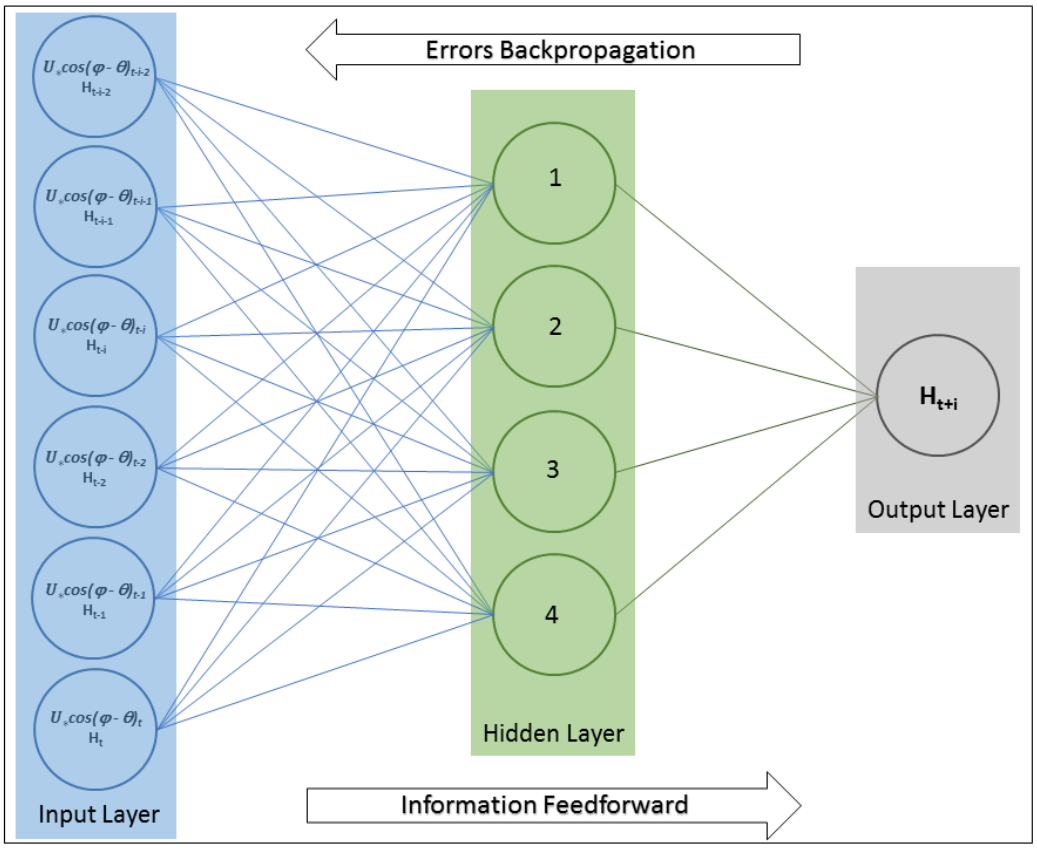

Fig. 2 — Schematic of NARX-based Model (B).

Without a well-recognized standard for selecting inputs lag times, trial and error approach had to be used. Optimal model performance was obtained through using lag time of 2 for both wind and wave inputs. For selecting optimal number of hidden neurons, also the trial and error approach had to be used, but with a limit that is based on the following criteria[47]:

$$N_H < 2N_I \quad \ldots (5)$$

where N_H represents the number of hidden neurons and N_I represent the number of inputs.

Based on Equations (3 and 4), and considering the lag time of 2, the number of hidden neurons (N_H), according to Equation (5), should be less than 24 for both models (A and B). Through trial and error, 4 was determined as the optimal number of hidden neurons.

Table (1) shows that for Model (A), with the same output, the modeling scheme (Equation 3) changes in terms of input (U_*,H) hours with the different forecasting horizons (i) according to the following equation:

$$H_{t+i} = f((U_*,H)_t,(U_*,H)_{t-1},(U_*,H)_{t-2},(U_*,H)_{t-i},(U_*,H)_{t-i-1},(U_*,H)_{t-i-2}) \quad \ldots (6)$$

The same scheme change applies to Equation (4) Model (B) input ($U_*\cos(\varphi-\theta), H$), Figure (2).

For both models (A and B), each input cell contains two data sets; corresponding to tapped-delay steps (1 and 2); of 3 consecutive hours each and these two data sets are separated by number of hours equivalent to the forecasting horizon (Table 1).

Performances of the two models were determined using three statistical parameters: Correlation Coefficient (r), Index of Agreement (I_a) and Mean Square Error (mse), given by the following equations:

$$r = \frac{\sum_n((t_n-\bar{t})*(y_n-\bar{y}))}{\sqrt{\sum_n(t_n-\bar{t})^2\sum_n(y_n-\bar{y})^2}} \quad \ldots (7)$$

$$I_a = 1 - \frac{\sum_n(y_n-t_n)^2}{\sum_n[|y_n-\bar{t}|+|t_n-\bar{t}|]} \quad \ldots (8)$$

$$mse = \frac{\sum_n(t_n-y_n)^2}{N} \quad \ldots (9)$$

where t represents the actual target (observed), y represents the model output, n represents the time step and N represents the total number of data points.

Results and Discussion

Figure 3 shows the variations in the overall performance for the two models, in terms of (r) and

Table 1 — Examples of the utilized modeling scheme for two forecasting horizons.

Forecasting Horizon (i)	Time (t)	Delay (d)	Input Hours	Output Hour
6	21	2	13 14 15	27
		1	19 20 21	
12	15	2	1 2 3	27
		1	13 14 15	

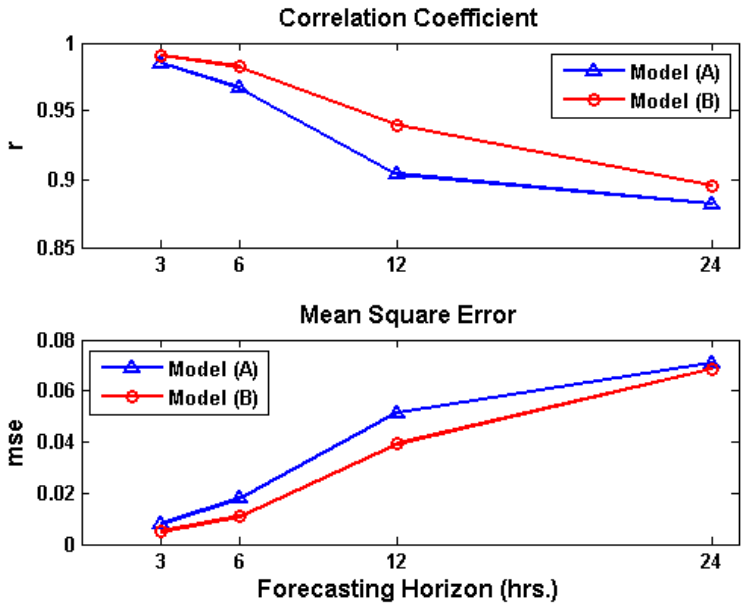

Fig. 3 — Variations of model overall performance in terms of correlation coefficient (r) [top panel] and mean square error (mse) [bottom panel] with forecasting horizons.

(*mse*), with the different forecasting horizons. The high performance obtained by the two models is mainly attributed to the high-resolution scheme that was adopted in this study (shown in Table 1 and Figure 2). The higher (*r*) and lower (*mse*) for model (B) in comparison with model (A), at all forecasting horizons, clearly indicated that model (B) outperformed model (A). This outperformance (Figure 3) has reached its maximum value at forecasting horizon of 12 hours for which model (B) has a much higher (*r*) and a much lower (*mse*) in comparison to those for Model (A). The models training and testing performances shown in Figure 4 in terms of (I_a), for the different forecasting horizons, also indicated the outperformance of model (B).

The comparisons between the observed (Target) and model predicted (Output) wave heights for forecasting horizon of 3 hours are shown in the form of scatter plots in Figures 5a and 5b for models (A) and (B), respectively. The scatter plots showed the good agreements between the observed and predicted wave heights with the majority of the points are in the proximity of the 45º line. The plots also showed, in terms of best fit lines that both models

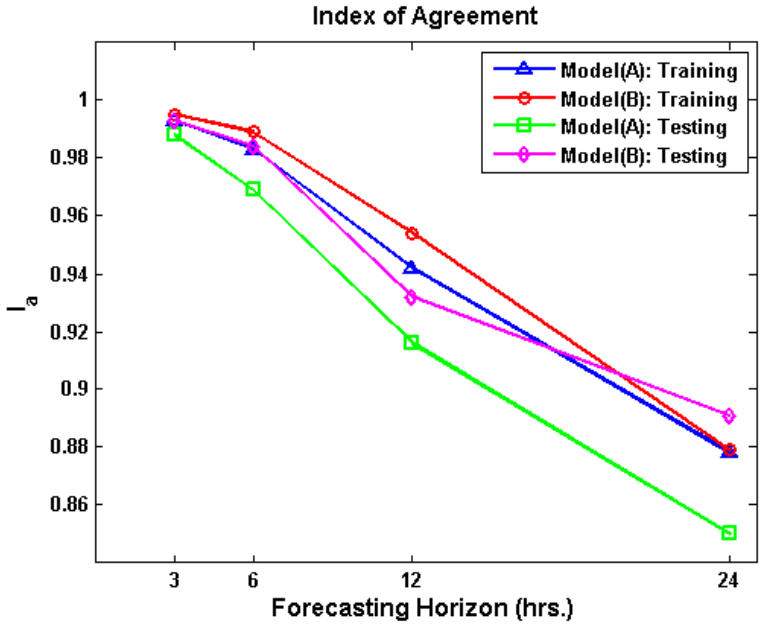

Fig. 4 — Variation of model training and testing performances in terms of index of agreement (I_a) with forecasting horizons.

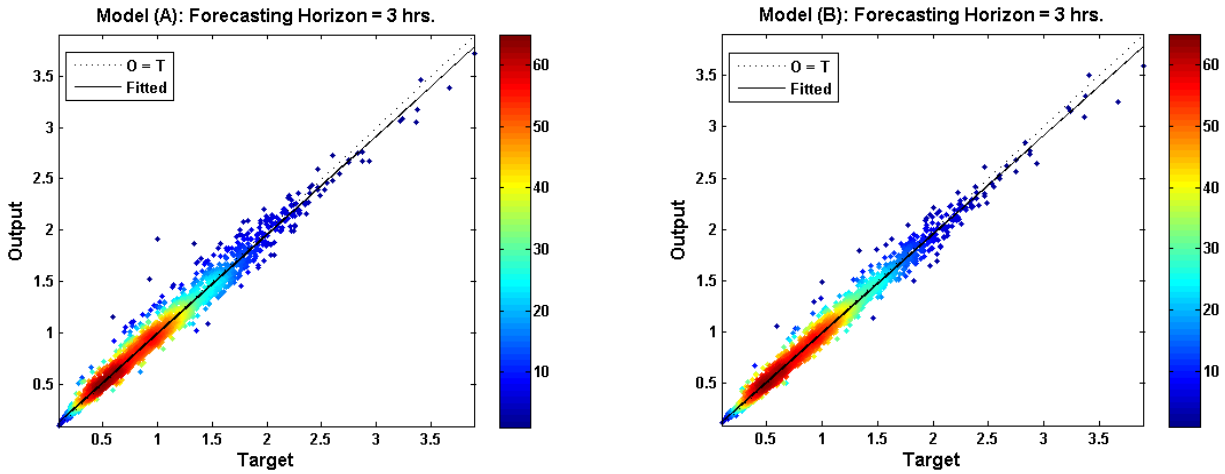

Fig. 5 — (a) Scatter plot comparison between Model (A) predicted (Output) and observed (Target) wave heights for 3 hours forecasting horizon. The colour bar indicates the number of collocated points; (b) Scatter plot comparison between Model (B) predicted (Output) and observed (Target) wave heights for 3 hours forecasting horizon. The colour bar indicates the number of collocated points.

slightly overestimated the low range wave heights and underestimated the high range wave heights. Furthermore, comparison between the two plots did not indicate a significant difference in performance between the two models. Figures 3 and 4 show that there is a slight difference in the performance of the two models in favor of Model (B).

For forecasting horizon of 6 hours, time series plots of observed (Target) and model predicted (Output) wave heights are given in Figures 6a and 6b for models (A) and (B), respectively. Comparison of the two plots shows that not only Model (A) overestimated a considerable number of peaks along the time series but also shows that Model (B) is producing a better match with the target time series. This was also indicated by the statistical comparisons shown in Figures 3 and 4.

The comparisons between the observed (Target) and model predicted (Output) wave heights for forecasting horizon of 12 hours are shown in the form of scatter plots in Figures 7a and 7b for models (A) and (B), respectively. The figures showed that both models overestimated the waves that were lower than 1 m height and underestimated the larger wave heights with the underestimation magnitude significantly increases as the wave height increases over 1 m. The comparison between the two Figures 7a and 7b shows that for model (B) the majority of the points are distributed much more closely to the best fit line indicating that Model (B) outperformed Model (A). This is also supported by the performance statistical comparisons given in Figures 3 and 4 for this forecasting horizon.

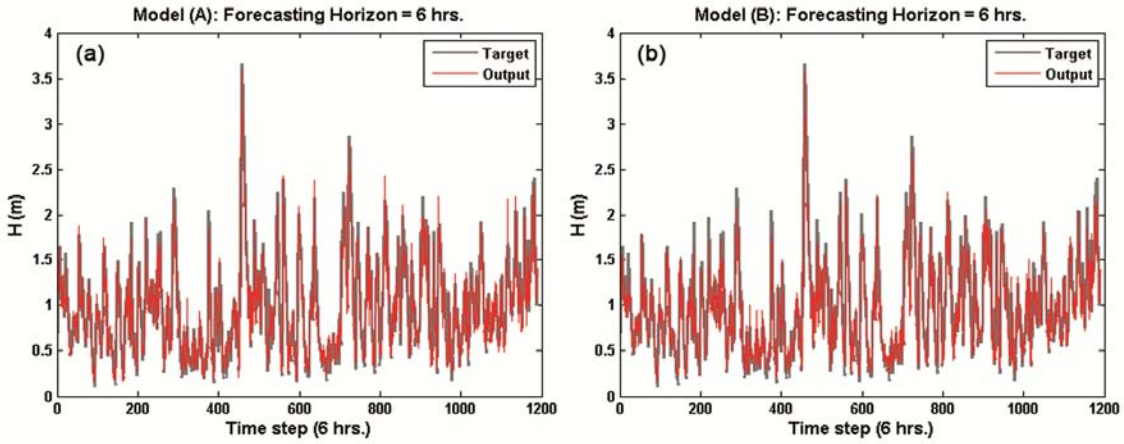

Fig. 6 — (a) Time series comparison between Model (A) predicted (Output) and observed (Target) wave heights for 6 hours forecasting horizon; (b) Time series comparison between Model (B) predicted (Output) and observed (Target) wave heights for 6 hours forecasting horizon.

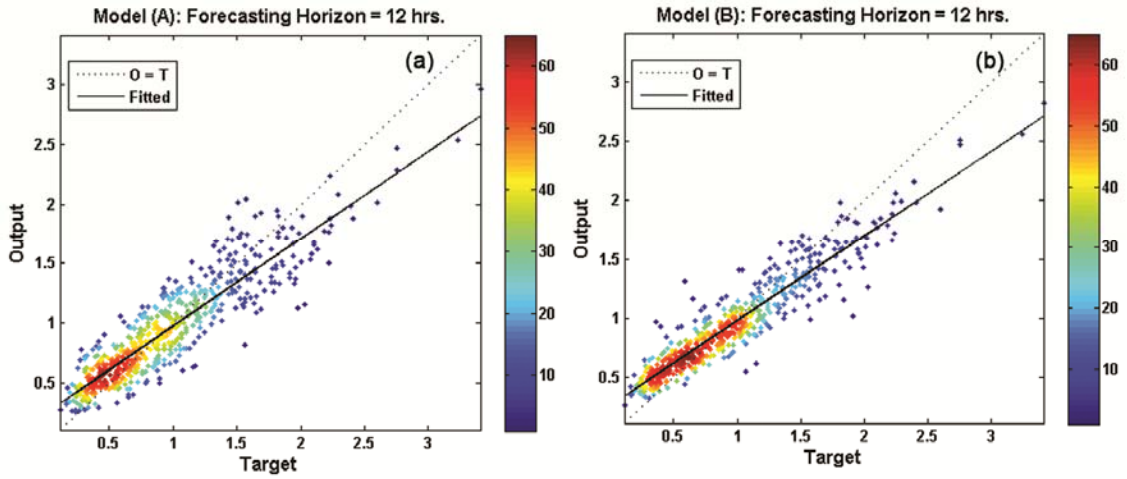

Fig. 7 — (a) Scatter plot comparison between Model (A) predicted (Output) and observed (Target) wave heights for 12 hours forecasting horizon. The colour bar indicates the number of collocated points; (b) Scatter plot comparison between Model (B) predicted (Output) and observed (Target) wave heights for 12 hours forecasting horizon. The colour bar indicates the number of collocated points.

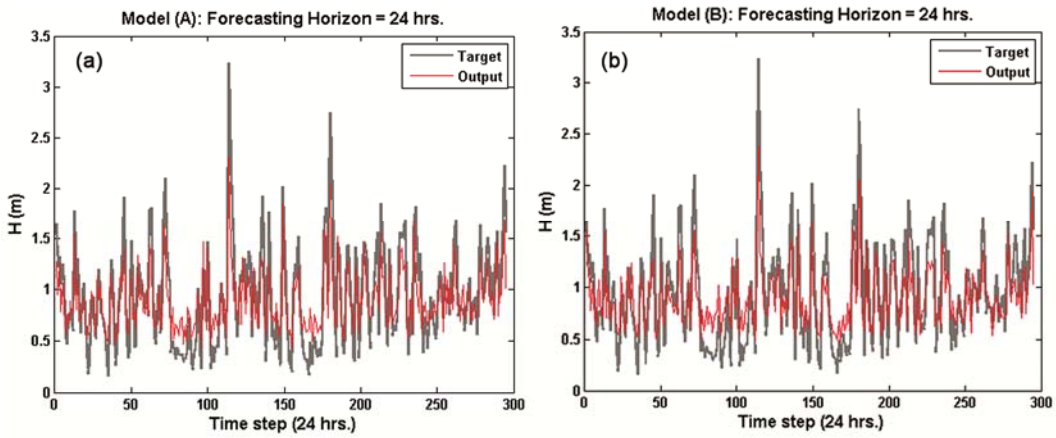

Fig. 8 — (a) Time series comparison between Model (A) predicted (Output) and observed (Target) wave heights for 24 hours forecasting horizon; (b) Time series comparison between Model (B) predicted (Output) and observed (Target) wave heights for 24 hours forecasting horizon.

For forecasting horizon of 24 hours, time series plots of observed (Target) and model predicted (Output) wave heights are given in Figures 8a and 8b for models (A) and (B), respectively. Comparison of the two plots shows that Model (A) overestimated a considerable number of peaks along the time series while Model (B) is showing a better match, in terms of peaks, between the two time series. Visually, it can be seen from the Figures 8a and 8b that both models (A and B) somewhat similarly over- and under-estimated the observed wave heights, however, a closer inspection shows that wave heights predicted by Model (B) have a pattern that is better matching the observed wave heights. This can be also indicated from Figures (3 and 4) which showed that the two models have a somewhat closer (*mse*) values but more differing (r) and (I_a) values.

Conclusion

Two NARX-based models have been developed for predicting waves observed at Eastern Central Red Sea for different forecasting horizons (3, 6, 12 and 24 h). The two models (A and B) differ by the inclusion of a wind and wave directions difference term as an input to model B only. Both models (A and B) predicted the observed wave heights with decreasing performances as the forecasting horizons increased. However, for all forecasting horizons, Model (B) has outperformed Model (A) indicating that the inclusion of the wind and wave directions difference input term have improved the quality of the predictions.

Acknowledgment

The author is thankful to King Abdullah University for Science and Technology (KAUST) and for National Data Buoy Center (NDBC) for making available the data collected by Met/Ocean buoy (NDBC: 23020).

References

1 USACE, *Shore protection manual*, 1(3), (U.S. Government Printing Office, Washington, DC, USA), 1984, pp. 140.

2 WMO, *Guide to wave analysis and forecasting*, 2nd ed. WMO-072, (Secretariat of the World Meteorological Organization, Geneva, Switzerland), 1998, pp. 159.

3 USACE, *Coastal engineering manual*, 2(2), (U.S. Government Printing Office, Washington, DC, USA), 2002, pp. 77.

4 Pierson, W.J., Moskowitz, L., A Proposed Spectral Form for Fully Developed Wind Seas Based on the Similarity Theory of S.A. Kitaigorodskii, *J. Geophys. Res.*, 69 (1964) 5181–5190.

5 Hasselmann, K., Barnett, T.P., Bouws, E., Carlson, H., Cartwright, D.E., Enke, K., Ewing, J.A., Gienapp, H., Hasselmann, D.E., Kruseman, P., Meerburg, A., Muller, P., Olbers, D.J., Richter, K., Sell, W., Walden, H., *Measurement of Wind Wave Growth and Swell Decay During the Joint North Sea Wave Project (JONSWAP)*, Report, (German Hydrographic Institute, Hamburg), 1973, pp. 95.

6 Hughes, S.A., *The TMA Shallow-Water Spectrum Description and Applications*, Technical Report CERC 84–7, (U.S. Army Waterways Experiment Station, Vicksburg, MS, USA), 1984, pp. 39.

7 Bouws, E., Gunther, H., Rosenthal, W., Vincent, C.L., Similarity of the Wind Wave Spectrum in Finite Depth Water, Part I—Spectral Form, *J. Geophys. Res.*, 90 (1985) 975–986.

8 Panchang, V. G., Bingyi, X., Demirbilek, Z., Wave Prediction Models for Coastal Engineering Application, in: *Developments in Offshore Engineering*, edited by John B. Herbich (Gulf Publishing Company, Houston, Texas, USA), 1999, pp.163-194.

9 Roland, A., Ardhuin, F., On the developments of spectral wave models: numerics and parameterizations for the coastal ocean, *Ocean Dynamics*, 64 (2014) 833–846.

10 The WAMDI Group, The WAM model - a third generation ocean wave prediction model, *J. Phys. Oceanogr.*, 18 (1988) 1775–1810.

11 Booij, N., Ris, R.C., Holthuijsen, L.H., A third-generation wave model for coastal regions 1. Model description and validation, *J. Geophys. Res.*, 104 (1999) 7649–7666.

12 Tolman, H., *User manual and system documentation of WAVEWATCH-III version 4.18*, Tech. Note. 316, NOAA / NWS / NCEP / OMB, 2014, pp. 282.

13 Siadatmousavi, S., Jose, F., Miot da Silva, G., Sensitivity of a third generation wave model to wind and boundary condition sources and model physics: A case study from the South Atlantic Ocean off Brazil coast, *Comput. Geosci.*, 90:B (2015) 57-65.

14 Van Vledder, G., Akpinar, A., Wave model predictions in the Black Sea: sensitivity to wind fields, *Appl. Ocean Res.*, 53 (2015) 161-178.

15 Beal, R. Jackson, T., *Neural Computing - An Introduction*, (Taylor and Francis Group, UK) 1990, pp. 256.

16 Jain, P., Deo, M.C., Neural networks in ocean engineering, *Ships Offshore Struc.*, 1(1) (2006) 25–35.

17 Jain, P., Deo, M.C., Real-time wave forecasts off the western Indian coast, *Appl. Ocean Res.*, 29:1-2 (2007) 72–79.

18 Mandal, S., Patil, S. G., Manjunatha, Y. R., Hegde, A. V., *Application of Neural Networks in Coastal Engineering – an Overview*, (The 12th International Conference of International Association for Computer Methods and Advances in Geomechanics IACMAG 1-6 October, Goa, India), 2008, pp. 1639-1645.

19 Deo, M.C., Naidu, C.S., Real time wave forecasting using neural networks, *Ocean Eng.*, 26 (1999) 191–203.

20 Deo, M.C., Jha, A., Chaphekar, A.S., Ravikant, K., Neural network for wave forecasting, *Ocean Eng.*, 28 (2001) 889–898.

21 Agrawal, J.D., Deo, M.C., On-line wave prediction, *Mar. Struct.*, 15 (2002) 57–74.

22 Makarynskyy, O., Improving wave predictions with artificial neural networks, *Ocean Eng.*, 31(5) (2004) 709-724.

23 Londhe, S. N., Panchang, V., One-day wave forecasts based on artificial neural networks, *J. Atmos. Ocean. Tech.*, 23(11) (2006) 1593-1603.

24 Makarynskyy, O., Pires-Silva, A.A., Makarynska, D., Ventura-Soares, C., Artificial neural networks in wave predictions at the west coast of Portugal, *Comput. Geosci.*, 31 (2005) 415–424.

25 Mandal, S., Rao, S., Raju, D. H., Ocean wave parameters estimation using backpropagation neural networks, *Mar. Struct.*, 18(3) (2005) 301-318.

26 Vimala, J., Latha, G., Venkatesan, R., Real time wave forecasting using artificial neural network with varying input parameter, *Indian J. Geo. Mar. Sci.*, 43(1) (2014) 82-87.

27 Deo M.C. Kumar N.K., Interpolation of wave heights, *Ocean Eng.*, 27(9) (2000) 907-917.

28 Paplińska-Swerpel, B., Paszke, Ł., Application of neural networks to the prediction of significant wave height at selected locations on the Baltic Sea, *Arch. Hydro-Eng. Environ. Mech.*, 3 (2006) 183-201.

29 Kamranzad, B., Etemad-Shahidi, A., Kazeminezhad, M., Wave height forecasting in Dayyer, the Persian Gulf, *Ocean Eng.*, 38(1) (2011) 248-255.

30 Kashikar, V. R., Mane, S. J., Artificial neural network: an effective tool for forecasting wave height, *Int. J. Eng. Res. Tech.*, 3(7) (2014) 744-747.

31 Diaconescu, E., The use of NARX neural networks to predict chaotic time series, *WSEAS Trans. Comp. Res.*, 3(3) (2008) 182-191.

32 Beale, M.H., Hagan, M.T., Demuth, H.B., *Neural Network Toolbox™ User's Guide*, (The MathWorks, Inc.) 2013.

33 Mandal, S., Prabaharan, N., Ocean wave forecasting using recurrent neural networks, *Ocean Eng.*, 33 (2006) 1401–1410.

34 Gopinath, D. I., Dwarakish, G. S., Wave prediction using neural networks at New Mangalore Port along west coast of India, *Aquatic Procedia*, (ICWRCOE'15), 4 (2015) 143 – 150.

35 Zubier, K. M., Abulnaja, Y. O., Al-Subhi, A. M., Development of an operational wave prediction system for the Red Sea: experimental phase, paper presented at *Offshore Arabia 2009 Conference*, Dubai, UAE, 2009.

36 Gharbi, S., *Numerical Wave Simulation in the Red Sea*, Master Thesis, King Abdulazizi University, 2012.

37 Ralston, D., Jiang, H. Farrar, J., Waves in the Red Sea: response to monsoonal and mountain gap winds, *Cont. Shelf Res.*, 65 (2013) 1-13.

38 Fery, N., Al-Subhi, A., Zubier, K., Bruss, G., Evaluation of the sea state near Jeddah based on recent observations and model results, *J. Oper. Oceanogr.*, 8(1) (2015) 1-10.

39 Langodan, S., Cavaleri, L., Viswanadhapalli, Y., Hoteit, I., The Red Sea: a natural laboratory for wind and wave modeling, *J. Phys. Oceanogr.*, 144(12) (2014) 3139-3159.

40 Langodan, S., Cavaleri, L., Viswanadhapalli, Y., Hoteit, I., Wind-wave source function in opposing seas, *J. Geophys. Res.-Oceans*, 120 (2015) 3751-6768.

41 Aboobacker, V.M., Shanas, P.R., Alsaafani, M.A., Albarakati, A.M., Wave energy resource assessment for Red Sea, *Renew. Energ.*, 114:A (2016) 46-58.

42 Langodan, S., Viswanadhapalli, Y., Hoteit, I., The impact of atmospheric Data assimilation on wave simulations in the Red Sea, *Ocean Eng.*, 116 (2016) 200-215.

43 Langodan, S., Viswanadhapalli, Y., Dasari, H. P., Kino, O., Hoteit, I., A high-resolution assessment of wind and wave energy potentials in the Red Sea, *Appl. Energ.*, 181 (2016) 244-255.

44 Langodan, S., Cavaleri, L., Pomaro, A., Viswanadhapalli, Y., Bertotti,L., Hoteit, I., The climatology of the Red Sea – part 2: the waves, *Int. J. Climatol.*, 37 (2017) 4518-4528.

45 Shanas, P.R., Aboobacker, V.M., Albarakati A.M., Zubier, K.M., Superimposed wind-waves in the Red Sea, *Ocean Eng.*, 138 (2017) 9-22.

46 Shanas, P.R., Aboobacker, V.M., Albarakati A.M., Zubier, K.M., Climate driven variability of wind-waves in the Red Sea, *Ocean Model.*, 119 (2017) 105-117.

47 Hecht-Nielsen, R., *Neurocomputing*, (Addison-Wesley) 1990, pp. 433.